Personalized Computer-Aided Diagnosis for Mild Cognitive Impairment in Alzheimer's Disease Based on sMRI and ^{11}C PiB-PET Analysis

FATMA EL-ZAHRAA A. EL-GAMAL[1,2], **MOHAMMED M. ELMOGY**[1], (Senior Member, IEEE),
ASHRAF KHALIL[3], **MOHAMMED GHAZAL**[4], (Senior Member, IEEE),
JAWAD YOUSAF[4], (Senior Member, IEEE), **XIAOLU QIU**[5], **HASSAN H. SOLIMAN**[1],
AHMED ATWAN[1], **HERMANN B. FRIEBOES**[2,7], **GREGORY NEAL BARNES**[6],
AND AYMAN S. EL-BAZ[2,8], (Senior Member, IEEE)

[1]Department of Information Technology, Faculty of Computers and Information, Mansoura University, Mansoura 35516, Egypt
[2]Department of Bioengineering, University of Louisville, Louisville, KY 40292, USA
[3]College of Technological Innovation, Zayed University, Dubai, UAE
[4]Department of Electrical and Computer Engineering, Abu Dhabi University, Abu Dhabi, UAE
[5]Jiangxi Children's Hospital, Nanchang, China
[6]Department of Neurology, University of Louisville Autism Center, Louisville, KY 40217, USA
[7]Center for Predictive Medicine, University of Louisville, Louisville, KY 40292, USA
[8]University of Louisville at AlAlamein International University (UofL-AIU), New Alamein City 48825, Egypt

Corresponding author: Ayman S. El-Baz (aselba01@louisville.edu)

ABSTRACT Alzheimer's disease (AD) is a neurodegenerative condition that affects the central nervous system and represents 60% to 70% of all dementia cases. Due to an increased aging population, the number of patients diagnosed with AD is expected to exceed 131 million worldwide by 2050. The disease is characterized by various clinical symptoms and pathological features that define three main sequential decline stages, namely, early/mild, intermediate/moderate and late/severe stages. Although it is considered irreversible, early diagnosis of AD is highly desirable to help preserve cognitive function. However, early diagnosis is difficult due to different factors, including the patient-specific development of AD. The main contribution of the proposed work is to present a personalized (i.e., local/brain regional) computer-aided diagnosis (CAD) system for early diagnosis of AD from two perspectives, functional and structural to assist diagnosis. In other words, the proposed system uniquely yields local/regional diagnosis by combining ^{11}C PiB positron emission tomography (^{11}C PiB PET), which provides functional diagnosis, with structural magnetic resonance imaging (sMRI), which provides structural diagnosis. To the best of our knowledge, this is the first work to combine sMRI and the ^{11}C PiB PET for local/regional early diagnosis of AD. The system processes the two modalities through a number of steps: pre-processing, brain labeling (parcellation), feature extraction, and diagnosis. A local/regional diagnosis is presented for each modality separately, followed by the final global diagnosis obtained by integrating the results from the two modalities. Evaluation of the proposed system shows average results of 97.5%, 100%, and 96.77% for accuracy, specificity, and sensitivity, respectively. With further development, it is envisioned that this system could contribute to the early diagnosis of AD in the clinical setting.

INDEX TERMS Alzheimer's disease, personalized diagnosis, MCI, ^{11}C PiB PET, sMRI.

I. INTRODUCTION

Dementia is a major problem challenging public health. Rather than being a single disease, dementia is defined as a symptom of different conditions that disrupt brain functionality (e.g., memory, language, and reasoning) [1]. Statistically, more than 44 million people around the world have dementia. By 2050, this number is expected to exceed 131 million [2]. The conditions and disorders related to dementia include Alzheimer's disease (AD), which represents sixty to seventy percent of all dementia cases in the elderly. AD is considered as one of the most well-known

The associate editor coordinating the review of this manuscript and approving it for publication was Alberto Cano.

F. E.-Z. A. El-Gamal *et al.*: Personalized CAD for MCI in Alzheimer's Disease Based on sMRI and ^{11}C PiB-PET Analysis

IEEE *Access*

neurodegenerative disorders that affect the central nervous system (CNS) [3]. Relying on the findings of the World Health Organization (WHO), the estimated increase of AD by 2050 in Asian, African, American, and European countries is 226%, 345%, 248%, and 90%, respectively [4].

Throughout its progression, AD evinces various clinical symptoms in addition to different pathological features. These symptoms classify AD into three sequential decline stages: early (mild), followed by intermediate (moderate), and ending with late (severe) [5]. Although the underlying process of AD is irreversible, early diagnosis in the early mild cognitive impairment (MCI) stage can provide a number of benefits [6]: (i) finding new therapeutic strategies to putatively modify the disease's effects and applying them most effectively at an early stage; (ii) preserving cognitive functions by slowing the disease's symptoms; and (iii) significant cost savings for both governments and patients in short as well as long-term care. Early diagnosis in the USA could save $7–$7.9 trillion in health and long-term care costs). However, early diagnosis remains a challenge. Reasons include the variable effect of the disease among its sufferers in addition to proper detection of pathological features 10–15 years before the appearance of the clinical symptoms [5].

Various tests are used for the purpose of assisting the diagnosis process of AD, including detection of brain biomarkers. Jack *et al.* [7] investigated the role of different types of brain biomarkers during the progression of the disease. The study showed that positron emission tomography (PET) amyloid imaging can reveal the earliest pathological features (i.e., amyloid beta (Aβ) deposits). Also, structural magnetic resonance imaging (sMRI) can uncover structural abnormalities throughout the stages of the disease. However, clinical implementation of PET amyloid imaging requires careful clinical interpretation, due to the possibility of misdiagnosis that can occur because of the similarity between AD-related Aβ abnormalities and other elevated Aβ levels in normal elderly subjects. The carbon-11-labeled Pittsburgh compound B (^{11}C PiB) tracer has been of considerable assistance in AD studies [8]. PiB radiotracer is a fluorescent analog of thioflavin T that aids in visualizing the prominent pathological features of AD and consequently helps to investigate the deterioration during the disease's stages [9]. Analysis via sMRI assists in non-invasively revealing structural changes during the disease progression. Also, the analysis shows the relation between both the growing risks of proceeding to AD and the atrophies which subsequently serve to predict future decline regarding healthy adult memory. Finally, volumetric analysis of this scanning modality can reveal essential changes to the size of brain regions, which is considered an effective assistance to diagnosis [9].

According to the aforementioned text, this paper's main contribution is to propose a personalized based (brain local/regional) computer-aided diagnosis (CAD) system of AD at its early stage from two different perspectives, functional and structural views. For this purpose, the ^{11}C PiB-PET and sMRI modalities were used to serve the functional and structural diagnosis goals, respectively. Utilizing these brain modalities was due to their prominent roles in the context of AD, as previously mentioned. Besides the modalities roles, to the best of the authors' knowledge, this is the first work that combines the sMRI and ^{11}C PiB-PET for AD's local/regional early diagnosis purpose. Also, presenting the local/regional diagnosis was to address the variable influence of AD among the disease's sufferers and therefore provide more assistance during the diagnosis procedure.

II. LITERATURE REVIEW

Instead of employing a single medical imaging modality, fusing multiple modalities has been explored to produce more informative results. Among the proposed attempts, the combined capabilities of sMRI and PET scans were utilized to help in the diagnosis of AD. Related studies have employed PET tracers other than ^{11}C PiB, such as a tracer called 2-^{18}F fluoro-2-deoxy-d-glucose (FDG). FDG is a metabolic substrate used with FDG-PET scans to measure glucose metabolism across brain regions and thus aid in the prediction of conversion from MCI to AD. For instance, Zhang and Shen [10] worked with a multi-modal data obtained from the sMRI, FDG-PET and cerebrospinal fluid (CSF) data to propose a Multi-Modal Multi-Task (M3T) learning. The aim of this presented learning methodology is to predict multiple variables from the utilized data that can be used for regression, through clinical variables, and for classification, through categorical variables. To achieve this goal, the presented method went through two stages, the first is multi-task feature selection for multiple variables from the utilized modalities, and then a multi-modal support vector machines (SVM) that fuses the selected features for multiple variables (regression and classification) prediction. The output of this methodology was in the form of Mini Mental State Examination (MMSE) as well as Alzheimer's Disease Assessment Scale-Cognitive Subscale (ADAS-Cog) as the clinical variables for regression and class labels as the categorical variables for classification. The proposed method was used for the estimation of the scores of the MMSE and ADAS-Cog as well as the classification labels in the normal controls (NC) *vs.* AD and NC *vs.* MCI groups. Additionally, it was used for the prediction of the changes in the 2-year MMSE and ADAS-Cog as well as the classification label in the classification task of MCI patients who converted to AD (MCI-C) *vs.* those who did not (MCI-NC). For the NC *vs.* MCI group they achieved an accuracy of 83.2%±1.5%, while it was 93.3% ± 2.2% for NC *vs.* AD and 73.9% ± 3.8% for MCI-C *vs.* MCI-NC task.

Gray *et al.* [11] presented a framework for multi-modality classification using the random forest (RF) algorithm to derive pairwise similarity measures for manifolds construction. For this purpose, sMRI, FDG-PET, CSF biomarker measures, as well as categorical genetic information are used. A combination of the obtained similarities from the multiple modalities is then performed to generate an embedding for feature based information encoding. Finally, this joint

IEEE Access

F. E.-Z. A. El-Gamal *et al.*: Personalized CAD for MCI in Alzheimer's Disease Based on sMRI and ^{11}C PiB-PET Analysis

embedding is used to perform a multi-modality classification. Evaluating the proposed framework between the healthy controls and MCI subjects showed an accuracy of 75% while it achieved 89% for the comparison between the healthy controls and AD patients.

Kim *et al.* [12] presented a classification method that utilized the integration of metabolism in FDG-PET scans along with the volume/thickness in sMRI. To achieve this multi-modal data integration, the proposed classification method used an automatic technique for the whole-brain analysis in addition to a graph-based semi-supervised learning (SSL) method. The comparison against a SVM classifier revealed superior results, especially with the volume/thickness measures. Additionally, values of the regions of interest (ROIs) that were extracted from the temporal lobe, hippocampus, and amygdala revealed that regional atrophy of the brain initially and extensively occurred in both the entorhinal cortex and hippocampus before spreading throughout the neocortex.

Jie *et al.* [13] utilized the multi-modality concept to improve the classification accuracy by presenting a manifold regularized Multi-Task Feature Selection (M2TFS) model based on MRI as well as PET data. For this purpose, the group lasso and Laplacian regularizers were applied. The group lasso regularizer was used for selecting a small number of features among the joint modalities, while the Laplacian regularizer was employed for the preservation of all the data, obtained from each modality, related to geometric distribution information. The proposed model was evaluated under supervised and semi-supervised learning methods. After supervised learning, the model had an accuracy of 95.03% for classification of AD *vs.* unimpaired NC, 79.27% for MCI *vs.* NC, and 68.94% for MCI-C *vs.* MCI-NC. In the semi-supervised run, the geometric distribution of the data yielded better discriminant feature selection. This observation was verified through the consistent improvement in the classification accuracy with the unlabeled samples in all three classification tasks.

Suk *et al.* [14] proposed a feature representation and system combining sMRI and FDG-PET scans to enhance the performance of AD/MCI diagnosis. Self-taught deep learning was used for this purpose, leading to efficient integration of complementary information obtained from MRI and PET scans during representation of the feature. Quantitatively, better results have been presented through the proposed system than the related method [15], [16]. The system showed the ability to visually reveal complex latent patterns, hidden in both modalities, in a hierarchical manner.

Lazli *et al.* [17] proposed a CAD system that consisted of a clustering stage followed by a classification stage. The aim of the clustering stage was to assess the white and gray matter as well as the cerebrospinal fluid volumes from noisy MRI and PET scans. For this purpose, fuzzy c-means was used followed by possibilistic c-means algorithm and ending up with the segmentation to delimit the tissue volumes of the brain. After the clustering process, the classification process

took place using SVM. Comparing the proposed system with the related approaches showed better results of the proposed work.

Mattsson *et al.* [18], addressed the diagnosis prediction task of AD through constructing least absolute shrinkage as well as selection operator with the ^{18}F-AV-1451 (tau) PET and the regional cortical thickness in addition to the subcortical volumes from the MRIs of the utilized scans. The evaluation of the proposed work implied that utilizing both modalities helped in partly capturing unique information that are relevant for clinical AD's reorientation.

Hao *et al.* [19] assisted in AD analysis through proposing a multi-modal method for feature selection with consistent metric constraint. First, the random forest strategy was utilized for each modality individually, VBM-MRI or FDG-PET, to calculate the similarity. Then, both regularization terms of the group sparsity and sample similarity constraint were utilized for objective function constraining from multiple modalities. Finally, the selected features obtained from different modalities were fused using multi-kernel SVM for final classification task. Evaluating the proposed system showed promising results.

Deep learning was employed by Li *et al.* [20] for prediction of missing patterns in PET scans by utilizing sMRIs. Three aspects were used to evaluate this system: (a) the prediction ability of the PET scans, (b) the accuracy of the classification against other methods, and (c) the effect on the accuracy of the combined features obtained from sMRI and PET scans. The system could achieve the prediction goals and attain better comparison results when testing sMRI, true and predicted PET, and MRI + PET scans. In particular, the feature combination of sMRI and PET scans showed improved classification accuracy. Liu *et al.* [21] also relied on deep learning to construct a CAD system composed of sparse stacked autoencoder (SAE) for input data representation and softmax regression layer for classification. The system was evaluated relative to the SVM classifier in two applications: binary classification (e.g., AD *vs.* NC or MCI *vs.* NC) and multiclass classification (i.e., NC, MCI-C, MCI-NC, and AD). In binary classification, the system achieved higher sensitivity in both cases and better overall classification accuracy of AD *vs.* NC. In multiclass classification, the system outperformed SVM in all classes except MCI-NC, where SVM mislabeled fewer cases.

Also, Suk and Shen [22] employed deep learning to propose their classification system that uses techniques of the automatic whole-brain ROI as well as Graph-based SSL method for multimodal integration of imaging data. For this purpose, the FDG and Florbetapir based PET scans where utilized along with the voxel-based morphometry (VBM) and FreeSurfer V5 data from sMRI. Evaluating the data showed best performance when integrating FDG and FreeSurfer data. Regarding the classification results, comparing the proposed graph-based SSL method and the SVM classifier showed, in general, better results of the proposed method except with Florbetapir data.

F. E.-Z. A. El-Gamal *et al.*: Personalized CAD for MCI in Alzheimer's Disease Based on sMRI and ^{11}C PiB-PET Analysis

IEEE *Access*

Despite the existence of various researches to serve the early diagnosis of AD, these studies yield a global diagnosis of AD and do not utilize ^{11}C PiB tracer when working with both sMRI and PET scans. Although the utilized PET based tracers in the previous work showed good results, ^{11}C PiB tracer has been found to help in revealing the earliest signs of the disease. This supports this tracer's role as an identifier in the early diagnosis stage of the disease [7]. Also, although the global diagnosis is an essential result in this context, proposing local/regional diagnosis could be more helpful to address the variability of the disease among patients which is a vital obstacle in front of the researchers in this field. This paper proposes a personalized based functional/structural CAD system to help diagnose AD at the early MCI stage. The novelty of this work is to present a local/regional diagnosis of AD from two different perspectives, a functional view using ^{11}C PiB-PET as well as a structural view using sMRI. These modalities are chosen due to their respective roles in early identification of the disease and related structural brain atrophy. Additionally, the proposed CAD system in this pilot study presents the capability for a final global diagnosis to provide an additional level of information.

III. MATERIALS, METHODS AND VALIDATION STRATEGY
A. MATERIALS
To evaluate the proposed system, we utilized a dataset from the Alzheimer's Disease Neuroimaging Initiative (ADNI) database (adni.loni.usc.edu) of subjects with both sMRI and ^{11}C PiB-PET scans. The initial launch of ADNI was in 2003 in the form of a public-private partnership under the leadership of Principal Investigator Michael W. Weiner, MD. The main goal of ADNI was to examine whether the serial sMRI, PET, other biological markers, and clinical and neuropsychological assessment can be combined to measure the progression of MCI and early AD. For more information about the protocols as well as the methods, the reader is referred to [23]. Data were obtained in accordance with the ADNI Data Use Agreement and with approval from the University of Louisville IRB (IRB protocol 19.0910). Additionally, ADNI data collection protocols were reviewed through the IRB at the Health System of Duke University and at each site. Prior to the collection of the data, all the subjects, as well as their legal representatives when appropriate, gave written informed consent [24].

In this study, a total of 81 sMRI and ^{11}C PiB-PET scans of 19 NC and 62 MCI subjects were utilized. It is noted that the utilized dataset was chosen since we intended to include only the subjects with both the sMRI and ^{11}C PiB-PET scans. Besides, it is noted that the scans that were initially pre-processed through ADNI were utilized in the proposed work. Despite the ADNI based initial pre-processing operations and to serve the targeted, personalized diagnosis goal, additional pre-processing steps were performed on these scans. The main aim of these extra pre-processing steps is to standardize the scans to a labeling atlas template to serve the brain regions' labeling task.

For the ^{11}C PiB-PET scans, the scans were co-registered, averaged, spatially oriented, intensity normalized, as well as smoothed through ADNI [25]. The ADNI based pre-processing operations on sMRI scans were in the form of multiplanar reconstruction (MPR) and a number of correction steps. These corrections start with gradwarping, an image-based system-specific correction of the geometry distortion that occurs because of the gradient non-linearity. Then, B1 calibration scans are utilized in a B1 non-uniformity to correct the intensity non-uniformity of the images. In this procedure of correction, a uniform sensitivity of the body coil is assumed. However, a poor signal-to-noise-ratio is showed when scanning the images by a body coil. Therefore, obtaining a head coil-based intensity inhomogeneity profile can be performed by dividing the smoothed version of the body coil image by the surface coil's smoothed one. The B1-corrected version of the head coil image can be attained via the multiplication of the uncorrected image and the estimated intensity profile [26]. Finally, the N3 histogram peak algorithm of sharpening is applied to reduce the images' intensity non-uniformity [27]. On anatomy, for the dependence elimination of the field estimate, an iterative approach is utilized for the estimation of the multiplicative bias field as well as the distribution of the true intensities of the tissue. Applying N3 on the MR data showed substantial improvement in the accuracy of the techniques used for the anatomical analysis such as tissue classification, cortical surface extraction, and registration [26].

Regarding the gold standard of diagnosis, the ground truth from ADNI, based on ADNI's classification criteria of AD related groups, was utilized. According to ADNI, the NC group was composed of subjects without any indications of having depression, cognition related impairments, or dementia. Patients in the MCI group were reported, by themselves, through an informant, or by a clinician, to suffer from memory concerns. These subjects did not show significant levels of impairment in other cognition domains or any signs of dementia. In order to determine the normality/abnormality of the participants' memory function, a part of the Wechsler Memory Scale (WMS) neuropsychological test was performed with respect to the participants' level of education as presented in Table 1. We focused on the MCI group with the goal to diagnose NC and MCI subjects regardless of whether the MCI subjects proceed to the AD stage, progressive MCI (pMCI), or remain as stable MCI (sMCI). Also, despite the ability of the ^{11}C PiB-PET scans to diagnose the

TABLE 1. Demographic data of the NC and MCI groups based scans that were used to evaluate the proposed framework.

(N = 81)	Average Age ± SD	Gender N (%)		WMS Logical Memory II results (based on years of education)		
		Male	Female	≥16 years	8-15 years	0-7 years
NC (19)	78.3 ± 5.01	11 (57.89)	8 (42.1)	≥ 9	≥ 5	≥ 3
MCI (62)	75.64 ± 7.89	42 (67.74)	20 (32.25)	≥ 8	≥ 4	≥ 2
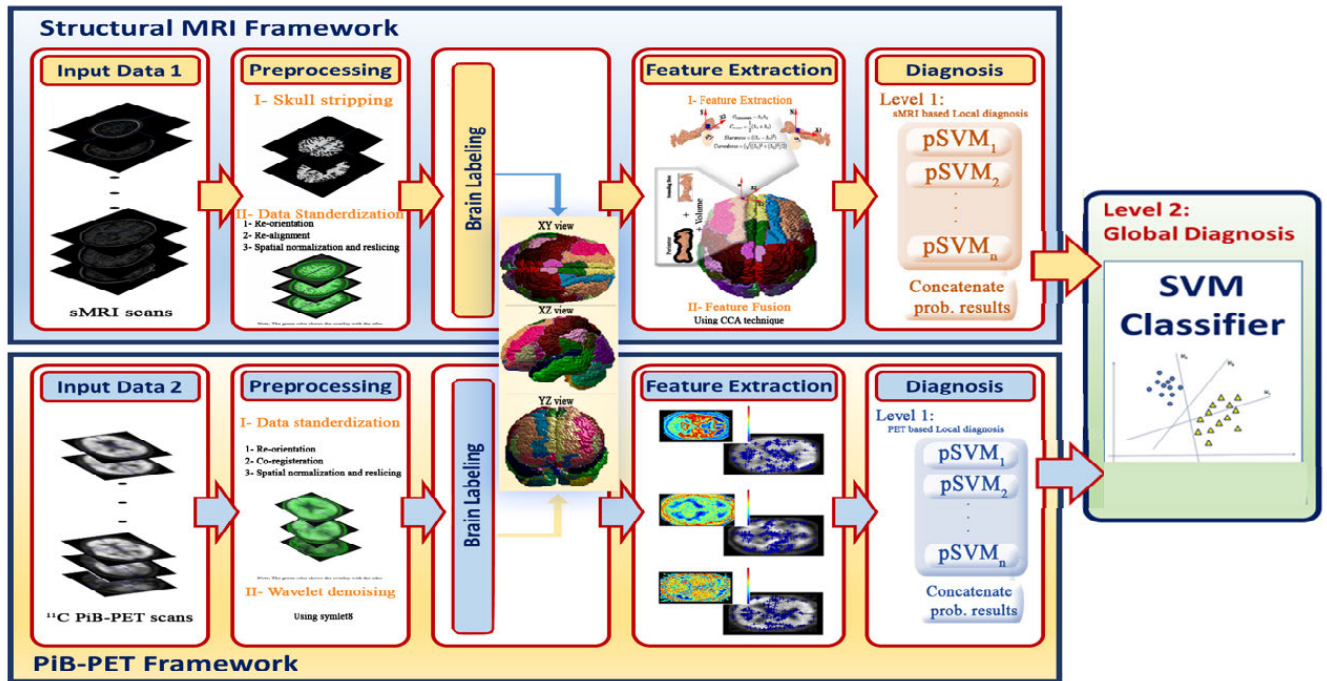
IEEE *Access*

F. E.-Z. A. El-Gamal *et al.*: Personalized CAD for MCI in Alzheimer's Disease Based on sMRI and ^{11}C PiB-PET Analysis

MCI subjects, here we utilized the sMRI along with PET scans in order to present the personalized diagnosis from two viewpoints for clinical evaluation.

B. METHODS

This paper builds a local/regional structural/functional computer based diagnostic system that aids in the personalized diagnosis process at the MCI stage of AD, the early stage of the disease. Thus, the proposed framework is mainly partitioned into two analysis stages, as presented in Fig. 1. First, the ^{11}C PiB-PET and sMRI scans are analyzed separately, and a local/regional diagnosis of the disease is obtained from each imaging modality for each anatomical brain region. Second, a final global diagnosis is produced by integrating the results from the two modalities. The proposed CAD system is described in detail in the following subsections.

1) ^{11}C PiB-PET AND sMRI SCANS PREPROCESSING

In addition to the ADNI's preprocessing operation on the utilized scans and in order to assess local/regional diagnosis, the scans need to be standardized first to the labeling atlas template's space, the Montreal Neurological Institute (MNI) space. This standardization yields anatomical brain labeling of the scans that serves the local/regional diagnosis. Therefore, the scans are processed in a number of steps: data re-orientation, co-registration, spatial normalization, and re-slicing (Algorithm 1).

Starting with the sMRI scans, before performing the standardization step, the scans undergo a skull stripping operation. To achieve this task, the scans are convolved with

their binary brain masks obtained from the ADNI. After performing this step, the sMRI scans, as well as the ^{11}C PiB-PET scans, are ready to be standardized. Starting with re-orienting the scans (i.e., sMRI and ^{11}C PiB-PET based scans), this operation is done with respect to the imaginary line between the anterior and posterior commissures (AC-PC line), and matching the orientation of the scan to that of the atlas template. Please note that re-orientation here to AC-PC line is differ than that of ADNI that re-orients the scans to a standard image grid that subsequently reorients the AC of the scan to be parallel to the AC-PC line.

Then, a least squares approach is used to calculate the six-degree-of-freedom, rigid body spatial transformation [28] to align the brain as closely as possible with the atlas. For this purpose: first, pick an sMRI scan (reference) and re-orient it to the line of AC-PC, and second, re-orient as well as re-align the target scans (i.e., the corresponding ^{11}C PiB-PET scan, and consequently the remaining ^{11}C PiB-PET scans, in addition to all the remaining sMRI scans) to the reference scan. Note that the second step is achieved through the composition of the re-orientation and rigid-body transformations. Mis-alignment is gauged with the mutual information based cost function and 7th degree B-spline interpolation method [29]. Note that the idea behind the cost function is to compare the registered image in order to measure their similarity. Among the cost function's methods there is the mutual information that addresses the structural similarity measurement between gray-scale images pairs in addition to perform cross-modality based registration between the images [30]. Also note that any of the sMRI scans can be

F. E.-Z. A. El-Gamal *et al.*: Personalized CAD for MCI in Alzheimer's Disease Based on sMRI and ^{11}C PiB-PET Analysis

IEEE*Access*

Algorithm 1 The Standardization Steps of Both ^{11}C PiB-PET and sMRI Scans

Input: Original ^{11}C PiB-PET, and sMRI scans with their corresponding masks.
Output: Standardized/atlas-matched scans.
Steps:

1) Strip the skull of the sMRI scans through convolving them with their masks obtained from ADNI database.
2) Re-orient both modalities to the AC-PC line through:
   a) Pick and re-orient one of the sMRI scans (reference scan) to the AC-PC line.
   b) Use the resulting re-oriented scan to re-orient the equivalent ^{11}C PiB-PET scan (and consequently the remaining sMRI scans).
   c) Apply the resulting re-orientation matrix of the PET scan to the remaining ^{11}C PiB-PET scans.
   d) Apply the rigid body transformation (i.e., translation, rotation, and mutual information cost function) to co-register both the sMRI and the ^{11}C PiB-PET modalities.
3) Spatially normalize as well as re-slice the scans to match the space of the atlas template (MNI space).
4) De-noise the ^{11}C PiB-PET scans using Algorithm 2.

Algorithm 2 The Steps of the Wavelet De-Noising Method

Input: Standardized/atlas-matched ^{11}C PiB-PET scans.
Output: De-noised standardized/atlas-matched ^{11}C PiB-PET scans.
Steps:

1) Select the mother wavelet, number of levels, and compute the forward wavelet transform of the inputted scans. In our work, the 'symlet8' mother wavelet has been selected with a single level of decomposition due to the low resolution of the ^{11}C PiB-PET scans.
2) Estimate the threshold and choose the shrinkage rule of how to apply the threshold in the detail coefficients using soft thresholding, where the coefficients under the threshold are deleted and the left are scaled, or hard thresholding, where the coefficients under the threshold are deleted and the left are remained unchanged. In our work, the soft thresholding was selected where the Stein's unbiased risk estimate rule was applied for selecting the threshold according to [35].
3) Use the modified coefficients to apply the inverse wavelet transform.

used as a reference scan as all the scans in ADNI database have broadly the same spatial orientation. Finally, note that one of the sMRI scans was used as a reference due to the high resolution of the sMRI as compared with the ^{11}C PiB-PET scans.

Then, spatial normalization of the scans to the atlas template, using the algorithm of Ashburner and Friston [31], are applied to the resulting re-oriented/re-aligned scans using full affine transformation to translate, shear, rotate, and scale the scans, in addition to apply the nonlinear deformations in order to achieve a precise outcome. After data standardization, the ^{11}C PiB-PET scans went through a de-noising operation to retain the details of the image while removing any artifact that could result during the image acquisition process or/and transmission [32]. For this purpose, the wavelet de-noising was used due to its good localization characteristic [33]. The wavelet de-noising steps applied in the proposed work are presented in Algorithm 2. Using symlet8 mother wavelet was due to its role as a compact support mother wavelet of least asymmetry and the highest number of the support width's vanishing moments. These aspects can consequently help in locally preserving the spatial aspects of the image [34].

2) BRAIN LABELING

After scan standardization, the next step is to label the brain regions using a detailed brain parcellation atlas as performed in [36]–[38]. The Automated Anatomical Labeling (AAL) atlas was selected for its fine level of detail. It parcellates the brain into 116 anatomical regions defined in part by the pattern of sulci in the MNI standard single subject's

brain, including 90 cerebral regions in both hemispheres and 26 cerebellar regions (nine in each cerebellar hemisphere and eight in the vermis) [39].

3) FEATURE EXTRACTION

At this stage, the discriminant features were extracted from the labeled regions taking into account the nature of both the disease and the utilized modalities. In the case of sMRI, the aim is to reveal characteristics of brain structure indicative of AD [40], that might not be directly detected at the MCI stage. Therefore, a number of geometric (i.e., bounding box, perimeter, and volume) and shape (Gaussian curvature, mean curvature, sharpness, and curvedness) features were calculated. The bounding box aims to determine the smallest rectangle that encloses the brain region producing a vector that contains the coordinates of the upper-left corner and the width of the obtained bounding box. The perimeter aims to produce a scalar that determines the distance around the region's boundary by finding the distance between the adjacent pair of pixels that surrounds the region's border. Here, the bounding box and perimeter were calculated for each slice of each region, and then the mean was calculated for the entire region's 3D volume. After extracting these features, to obtain the volume as well as the shape features, a reconstruction process of each region is performed. The marching cubes (MC) algorithm was applied because it is known to be the best method for isosurface extraction due to its ability to produce high-resolution results. More details about the reconstruction using MC algorithm can be found in [41] whereas [42], [43] provide utilization examples of isosurface

IEEE Access

F. E.-Z. A. El-Gamal *et al.*: Personalized CAD for MCI in Alzheimer's Disease Based on sMRI and ^{11}C PiB-PET Analysis

Algorithm 3 Extraction of the Shape Based Features From the sMRI Scans

Input: Each labeled sMRI based anatomical brain region.
Output: shape based features (curvatures, sharpness, and curvedness).
Procedures:

1) Use the volume lattice to define cubes (C_l) where the cubes vertices of the corner V_l are defined through the points ($P(x_i, y_j, s_k)$) of the lattice for column $x_i(\forall_i)$, $y_i(\forall_j)$ and slice $S_k(\forall_n)$:n is the number of slices.

2) In a sequential vertex by vertex manner and throughout the rows of the dataset, build a fecetized isosurface. During this, mark each V_i when it has a greater than or equal value compared to the isovalue α and keep the remaining vertices unmarked.

3) Define the "active" cube that is the cube where the isosurface intersects with its edge E_j that terminated by a marked vertex V_jm and an unmarked vertex V_ju. There are different scenarios, specifically speaking 256 scenario (2^8), to mark the cube since each of the cube's eight vertices can be either marked or unmarked. Each of these scenarios encodes a pattern for the cube-isosurface intersection. The facetization information of the intersecting isosurface can be obtained through a prior built look-up table that contains the intersection topologies. To estimate the isosurface-edge intersection location $I = (I_x, I_y, I_s)$, the linear interpolation is applied as:

$$I(x, y, s) = V_{m(x,y,s)} + \rho(V_{u(x,y,s)} - V_{m(x,y,s)})$$

where: $\rho = \frac{\alpha - L_m}{L_u - L_m}$, L_m and L_u are the scalar values V_m as well as V_u, respectively.

4) Utilize the extracted isosurface, triangulated mesh, to calculate the curvature based features through the following equations:

$$C_{\text{Gaussian}} = \lambda_1 \lambda_2 \tag{1}$$

$$C_{\text{mean}} = \frac{1}{2}(\lambda_1 + \lambda_2) \tag{2}$$

$$\text{Sharpness} = (\lambda_1 - \lambda_2)^2 \tag{3}$$

$$\text{Curvedness} = \sqrt{(\lambda_1^2 + \lambda_2^2)/2} \tag{4}$$

where λ_1 and λ_2 are the principal curvatures, or eigenvalues of the shape operator, estimated at each node of the mesh.

in neuroimaging context. Algorithm 3 presents the steps of extracting the shape features utilizing the MC algorithm [44]. Beside these shape features, the volume was calculated for each reconstructed region as well since it is considered as a well-known, cross-sectional quantitative metric of AD [45]. Thus, rather than relying the sMRI features on the volume alone, the volume was utilized in conjunction with the other aforementioned shape and geometric features to avoid bias

and to obtain more precise results through revealing as much as possible information from the scans.

To maximize the representative information, a feature fusion procedure, relying on the canonical correlation analysis (CCA) technique, was applied to the extracted features [46]. CCA was chosen due to its role in addressing the relationship between two variable sets by finding the linear combinations that maximize the pair-wise correlations between the sets. In this study, the CCA was utilized sequentially by fusing two features at a time until arriving at the final vector of the fused features.

For ^{11}C PiB-PET scans, each region was analyzed with the scale-invariant blob detection method, employing laplacian of Gaussian (LoG) filters with automatic scale selection [47]. Blob detection aims to highlight primarily spherical structures (i.e., blobs) from the images and present them as a feature where the blob is a local minimum or maximum intensity with a radially symmetric distribution [48]. Depending on the blob characteristics, the extracted blobs could be used to detect AD-related abnormalities, since AD has a high significant retention of PiB in brain regions that have increased $A\beta$ plaques [49]. Relying on this fact and for each region, a vector of blobs that correspond to the local maxima will be targeted through the LoG detector with automatic scale selection.
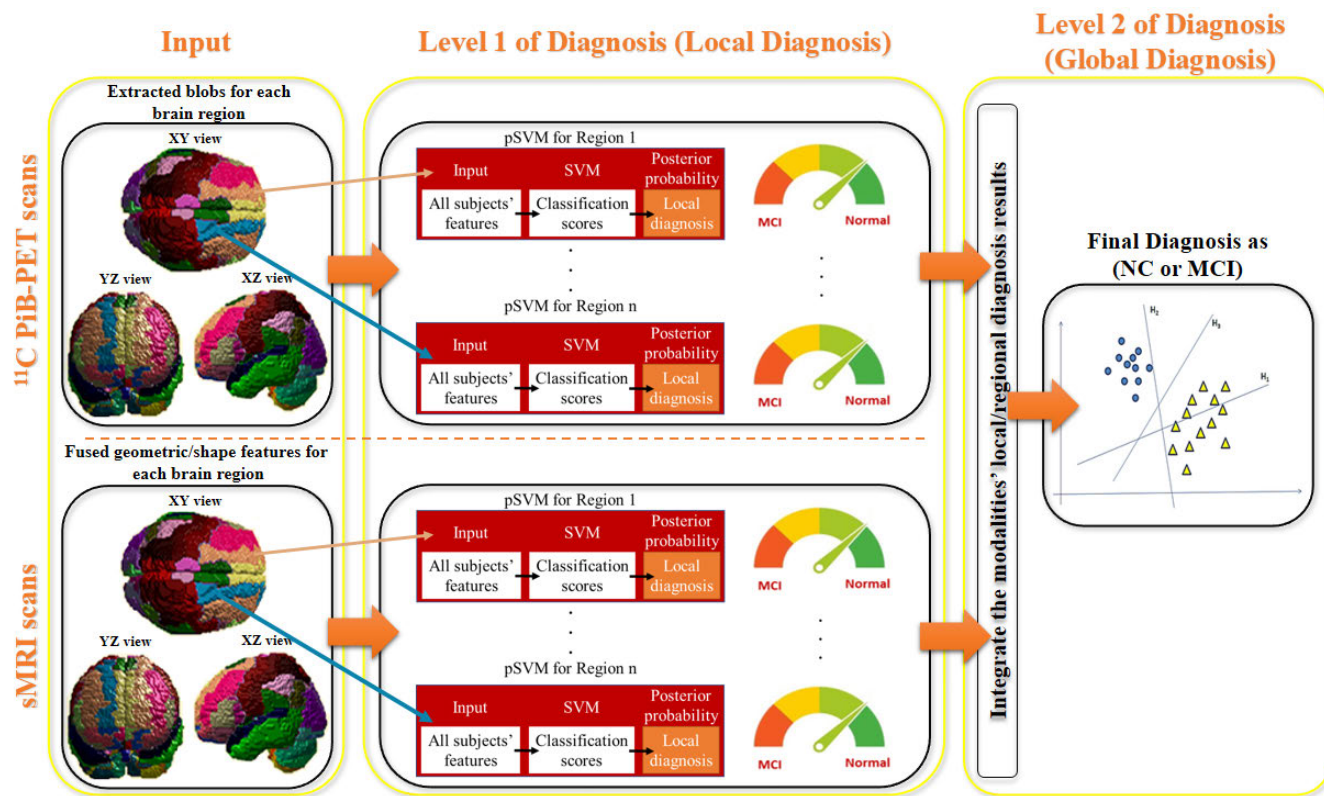
4) DIAGNOSIS

After extracting regional features from the sMRI and ^{11}C PiB-PET scans, the features were used to construct two levels of diagnosis, 1) local/regional diagnosis followed by 2) a final global diagnosis. To achieve the target of the first level, for each of the utilized modalities, separate 116 probabilistic SVM (pSVM) were constructed for each of the labeled brain regions. The aim of these separate pSVM was to produce a probabilistic brain regional based diagnosis from each modality point of view. These probabilistic results reflect the severity of AD in each brain region separately. Then, the second diagnosis level was constructed to classify each subject as belonging to the NC or MCI group. For this purpose, the maximum of the probabilistic results from the two modalities, for all the brain regions, were obtained and input to a standard SVM to produce the final diagnosis of the subject. Note that the first diagnosis level is brain regional based diagnosis where the 116 labeled regions obtained through AAL atlas were used to construct the separate 116 pSVM. On the other hand, the second diagnosis level is subject based diagnosis, where the labels of AD related stages (i.e., NC and MCI) were used to construct the standard SVM. The idea of the proposed diagnosis levels is presented in Figure 2.

C. VALIDATION STRATEGY

The proposed CAD system was implemented using MATLAB. The preprocessing operations of data re-orientation, co-registration, spatial normalization, and re-slicing were performed using the SPM 12 toolbox of MATLAB [28], whereas the brain labeling task was accomplished through

F. E.-Z. A. El-Gamal *et al.*: Personalized CAD for MCI in Alzheimer's Disease Based on sMRI and ^{11}C PiB-PET Analysis

IEEE *Access*

FIGURE 2. Proposed two diagnosis levels (i.e., local followed by global diagnosis) and their relation with the inputted extracted features from the both modalities.

the xjView toolbox [50]. Then, the region-based feature extraction was performed. Regarding sMRI, the result of feature extraction process produced a fused feature vector of the geometric and shape features. While for the ^{11}C PiB-PET scans, the result produced a vector of the extracted blobs. Later, two diagnosis levels were constructed to present a local/regional based diagnosis followed by a final global (i.e., subject based) diagnosis. In the first level, for each of the 116 AAL atlas based brain regions in each modality individually, a separate pSVM was utilized to produce a probabilistic result that reflects the severity of the disease in the region. Then, the maximum of the obtained probabilistic results for all the regions from the both modalities were obtained for each subject and inputted to a standard SVM in the second level to determine the final global diagnosis of belonging to the NC or MCI groups.

Two types of experiments were used to validate the proposed work, the classification analyses, as well as the regional diagnosis and putative neurocircuits. In the first type, the performance comparison between the proposed SVM-based system and state-of-the-art classifiers was performed. Therefore, two validation methods (i.e., leave-one-subject-out (LOSO) and K-fold cross-validation, with $K \in \{2, 4, 10\}$) were utilized. In general, for this purpose and after dividing the dataset into the validation method required groups (e.g., 10 groups for $K = 10$), each unique group of subjects will

be used, in a loop manner of the groups' number, for testing. In contrast, the remaining groups will be used to train and fit the model on them before evaluating it on the testing group. Then, before going to the next iteration of the loop, the evaluation score will be retained, and the model will be discarded. After ending the loop, the iterations' scores will be used to evaluate the model. Note that the utilization of several different K was in order to check for overfitting that might occur because of the imbalanced dataset due to the restriction to subjects with both sMRI and ^{11}C PiB-PET scans.

In this paper, the process goes into two main steps. First, for each modality, the training data will be used to train each of the brain regions' separate SVM models that will be applied then on the testing data. This step is probabilistic results for each of the 116 regions for the training groups and testing group from both modalities perspectives. Second, the maximum of obtained regions' probabilistic results, from both modalities, will be used to train the standard SVM model that will consequently be tested on the testing group's maximum probabilistic results regions obtained from both modalities. The result of this step reflects the final subject-based result. To evaluate the classification's performance according to these methods, three evaluation metrics are utilized: accuracy, specificity, and sensitivity. On the second type, the regional diagnosis, and putative neurocircuits, the Pearson correlation coefficient was used that presents a statistical measure of

the relationship strength relationship between the two tested groups.

IV. EXPERIMENTAL RESULTS

A. CLASSIFICATION ANALYSES

Starting with the analysis of the classification results and before going through the comparison of the proposed work with the state-of-the-art methods, the classification performance, using LOSO, of each of the utilized modalities is calculated as shown in Table 2. In addition to these results, the table shows the results obtained after fusing the two modalities. Please note here that the linear kernel was used to construct each modality subsystem and accordingly the integrated system due to its superior performance compared to other SVM kernels.

TABLE 2. The classification performance of [11]C PiB-PET scans, sMR images, and their fusion using LOSO validation method.

	Accuracy	Specificity	Sensitivity
[11]C PiB-PET scans	100	100	100
SMR images	83.95	42.11	96.77
Integration of both modalities	100	100	100

TABLE 3. Comparison of the classification performance between the proposed linear-SVM and representative state-of-the-art classifiers using LOSO and K-fold methods.

		LOSO	$K = 2$	$K = 4$	$K = 10$
NB	ACC	93.83	98.78	100	98.75
	Spec.	84.21	94.74	100	94.74
	Sens.	96.77	100	100	100
DL	ACC	93.83	85.21	92.5	91.39
	Spec.	73.68	57.89	73.68	73.68
	Sens.	100	93.55	98.39	96.77
DT	ACC	92.59	100	100	100
	Spec.	68.42	100	100	100
	Sens.	100	100	100	100
RF	ACC	100	96.31	98.75	98.75
	Spec.	100	89.47	94.74	94.74
	Sens.	100	98.39	100	100
Proposed system	**ACC**	**100**	**97.5**	**100**	**100**
	Spec.	**100**	**100**	**100**	**100**
	Sens.	**100**	**96.77**	**100**	**100**

NB: naive Bayes, **DL:** deep learning, **DT:** decision tree, **RF:** random forest.

Then, as mentioned above, to evaluate the diagnostic performance, the performance of the proposed functional/structural SVM-based CAD system was compared to state-of-the-art classifiers, namely naïve Bayes (NB), random forest (RF), deep learning (DL), and decision tree (DT). The LOSO and K-fold cross-validation methods were used to perform the comparison task as shown in Table 3. The architecture of the DL comparison classifier was a multi-layer feed-forward artificial neural network (ANN), which was trained with stochastic gradient descent using back-propagation. It is important to note that when constructing the applied classifiers, the parameters were optimized to produce final performance results as follow: (i) for DT, the maximum depth of a tree was 2; (ii) for RF the optimal number of trees was found to be 60 while their maximum depth was 4; (iii) for SVM, the kernel gamma was 0.01 and the optimal complexity constant, the misclassification tolerance, was 10.

B. REGIONAL DIAGNOSIS AND PUTATIVE NEUROCIRCUITS

The proposed system helps to determine the disease progression in the brain regions from structural and functional views. As shown in Fig. 4, the colormap reflects the severity of the disease in each region separately starting from the white color that means unaffected region to dark red which is a fully indicative of MCI in the region and the colors' range between these two colors to indicate the probability between these ranges. According to these informative colors, the two illustrated examples (the NC and MCI examples) show how the disease influence starts to appear in the [11]C PiB-PET scans while it does not yet appear in the sMRI

(i.e., the orange, red and dark red colors in PET scans *vs.* white or light yellow colors in MRI). These obtained results are supported by the fact that the disease's pathological features start 10–15 years before the clinical symptoms. This fact can help justify the appearance of some affected regions in the NC that, in turn, may indicate that these regions started to be influenced by the disease and accordingly represent an alert to the specialists to deal with them. Besides, they are showing the influence in the [11]C PiB-PET scans, although sMRI doesn't show that much influence could be supported by the findings of Jack *et al.* [7] study.

As mentioned previously, this study showed that the [11]C PiB-PET scans represent an indicator of the early signs of AD, the earliest pathological features of AD. In contrast, the effect of the disease can be shown later in the sMRI. This conclusion can also be seen in Fig. 3. As shown in Fig. 3, a comparison of the number of normal regions in the sMRI and [11]C PiB-PET scans indicates that most of the regions in the NC subjects in the sMRI scans are normal. In contrast, more regions for the same subjects in the [11]C PiB-PET scans showed impairment effects. In this case, the [11]C PiB-PET scans of these MCI subjects were more sensitive for detecting impairment than the corresponding sMRI scans.

The results of the local diagnosis and fusion further validate the proposed approach. Pearson correlations identify 17 significant regions in structural MRI data which have modest to high negative or positive correlates with 4–7 connected brain regions only in MCI subjects (Table 4). Similarly, [11]C PiB-PET scans identify 5 regions with moderate to very strong correlates with 4-8 connected brain regions, again only in MCI subjects (Table 5). Finally, at the global diagnosis

F. E.-Z. A. El-Gamal et al.: Personalized CAD for MCI in Alzheimer's Disease Based on sMRI and ^{11}C PiB-PET Analysis

IEEE Access

TABLE 4. Significant regions identification in MCI Subjects using Pearson correlations on the sMRI Data.

Brain Region[*]	CBN[**]	Range of Pearson r values	Range of p values
Left Amygdala	4	-0.69 to +0.43	0.0004 to 4.67×10^{-10}
Right Angular Gyrus	4	-0.52 to +0.41	0.001 to 1.53×10^{-5}
Right Caudate	4	-0.48 to +0.68	0.0005 to 1.43×10^{-9}
Left Cerebellum 6 Lobule	5	-0.44 to +0.44	0.001 to 2.76×10^{-4}
Left Cerebellum Crus 1 Lobule	5	-0.52 to +0.64	0.0005 to 1.89×10^{-8}
Right Cerebellum Crus 2 Lobule	5	-0.56 to +0.50	0.0005 to 1.40×10^{-6}
Left Mid Cingulum	7	-0.45 to +0.52	0.001 to 1.31×10^{-5}
Left Cuneus	5	-0.84 to +0.69	0.001 to infinity (0)
Left Inferior Frontal Triangularis Gyrus	5	-0.55 to +0.41	0.0008 to 2.51×10^{-6}
Left Mid Orbital Frontal Gyrus	5	-0.45 to +0.75	0.0002 to 2.21×10^{-12}
Right Mid Frontal Gyrus	5	+0.41 to +0.47	0.001 to 1.06×10^{-4}
Left Medial Superior Frontal Gyrus	4	-0.44 to +0.67	0.001 to 1.40×10^{-9}
Right Superior Frontal Gyrus	7	-0.43 to +0.55	0.0004 to 9.11×10^{-7}
Right Hippocampus	4	-0.72 to +0.41	0.0006 to 2.67×10^{-11}
Right Lingual Gyrus	5	+0.40 to +0.80	0.001 to 5.77×10^{-15}
Right Paracentral Lobule	4	-0.52 to 0.55	0.0002 to 3.89×10^{-6}

[*] Brain region with > 3 potentially connected other areas with a Pearson r value at < or = 0.001.
[**] CBN: Number of Connected Brain Regions.
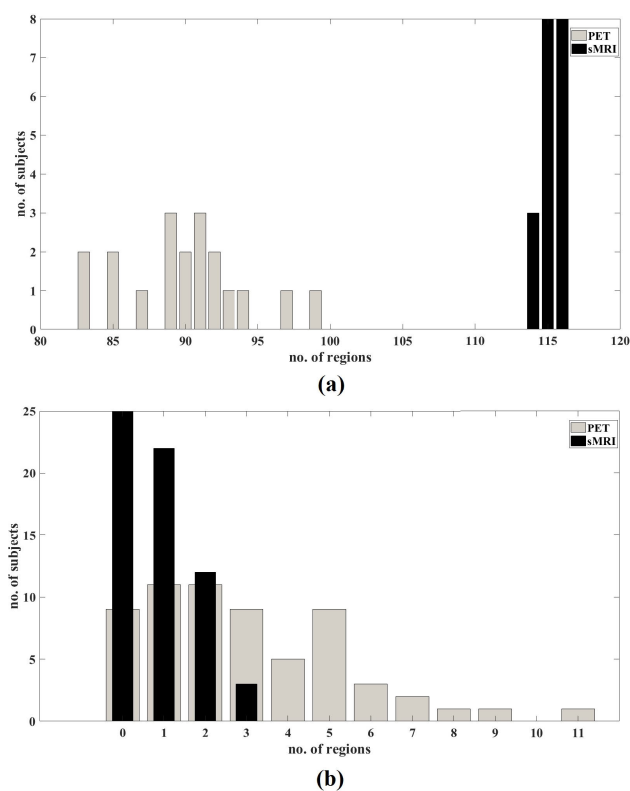
FIGURE 3. Comparison between ^{11}C PiB-PET and sMRI scans where: (a) compares the number of normal regions (x-axis) in the both modalities with respect to the NC subjects (y-axis), and (b) compares the number of affected regions (x-axis) in the two modalities with respect to the MCI subjects (y-axis).

stage, fusion data reveals 5 regions previously implicated in MCI and AD with moderate to high positive correlated with 4–5 connected brain regions (Table 6). As shown in Fig. 4, the examples illustrate the variable influence of the disease in particular brains. This approach could be used to identify the individual neurocircuits in the personalized diagnosis/

treatment of the disease as well as in analysis studies that seek to uncover the ambiguity that surrounds AD.

V. DISCUSSION

The shape, composition, and function of the brain, including neocortex, subcortical structures, and cerebellum, as measured by imaging modalities plays a crucial role in the diagnosis of neurodegenerative diseases. Depending on imaging variability and variable neuropathology during the progression of AD, a CAD system should be able to detect this variability and discriminate between NC and MCI groups. Additionally, a CAD system should be able to identify impaired neurocircuits in the imaged brain which may need further treatment even if those circuits are just mildly affected.

Starting with each of the utilized modalities subsystems results, Table 2 highlights the superior performance of ^{11}C PiB-PET scans in addressing the early signs of disease as mentioned in Jack et al. [7]. Further, the results illustrate the utility of sMRI, as validated with related work that achieved an accuracy of 85% [51] or 70.19% [52]. Although the performance results of the ^{11}C PiB-PET scan and the integration of both modalities were similar, the proposed system is still able to present the diagnosis of the disease from both structural and functional perspectives. This capability represents the main contribution of the proposed CAD system.

Then, a comparison of the proposed functional/structural SVM-based CAD system was performed where the comparison results are presented in Table 3. As shown in the table, the LOSO and K-fold, with K = 2, 4, and 10, validation methods were utilized. Besides using these validation methods for the comparison purpose, these methods helped in assuring that there is no overfitting in the obtained results. According to the table results, the presented functional/structural SVM-based CAD system yields better results than the compared classifiers. These results can be explained through the power of the features to provide a linear separation

IEEE Access

F. E.-Z. A. El-Gamal *et al.*: Personalized CAD for MCI in Alzheimer's Disease Based on sMRI and ^{11}C PiB-PET Analysis

TABLE 5. Significant regions identification in MCI subjects using pearson correlations on the ^{11}C PiB-PET data.

Brain Region*	CBN**	Range of Pearson r values	Range of p values
Left Calcarine Gyrus	4	+0.42 to +0.49	0.0006 to 4.96 x 10^{-5}
Right Cerebellum 10 Lobule	4	+0.42 to +0.69	0.0006 to 2.54 x 10^{-10}
Left Cerebellum 10 Lobule	6	+0.46 to +0.62	0.0001 to 5.85 x 10^{-8}
Left Cerebellum 3 Lobule	8	+0.44 to +0.67	0.0003 to 1.93 x 10^{-9}
Right Olfactory Gyrus	6	+0.53 to +0.98	1.13 x 10^{-5} to Infinity(0)

* Brain region with > 3 potentially connected other areas with a Pearson r value at < or = 0.001.
** CBN: Number of Connected Brain Regions.

TABLE 6. Significant regions identification in MCI Subjects using Pearson correlations on the fusion of ^{11}C PiB-PET and sMRI Data.

Brain Region*	CBN**	Range of Pearson r values	Range of p values
Left Calcarine Gyrus	5	+0.42 to +0.48	0.0007 to 6.90 x 10^{-5}
Left Caudate	5	+0.41 to +0.54	0.0009 to 5.60 x 10^{-6}
Left Cerebellum 3 Lobule	4	+0.44 to +0.65	0.0003 to 1.12 x 10^{-8}
Right Medial Superior Frontal Gyrus	4	+0.42 to +0.55	0.0007 to 3.36 x 10^{-6}
Right Parahippocampal Gyrus	4	+0.45 to +0.70	0.0002 to 1.64 x 10^{-10}

* Brain region with > 3 potentially connected other areas with a Pearson r value at < or = 0.001.
** CBN: Number of Connected Brain Regions.
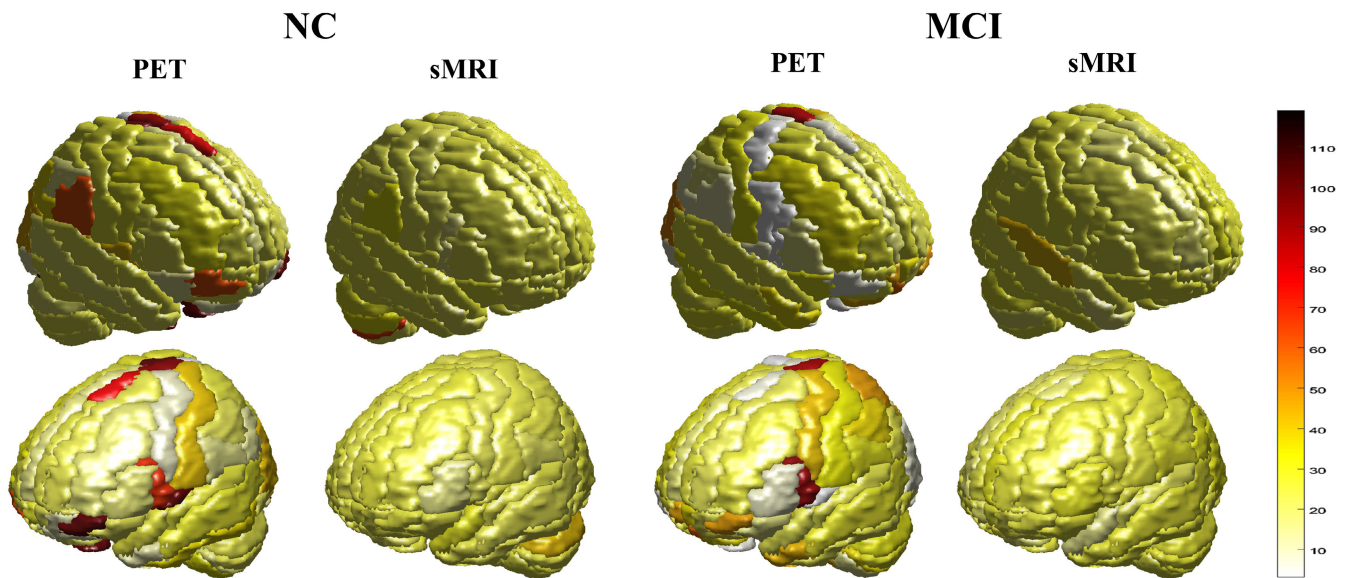
FIGURE 4. Visualization examples of the local/regional diagnosis for an NC subject and an MCI with two rendering volumes for each subject, one for the functional view (through the ^{11}C PiB-PET scan) and the other for the structural view (through the sMRI scan). The severity of the disease is represented via the colormap where these colors are reflected in each of the 116 region of the subjects' volumes to indicate the severity of the disease in every region from each of the utilized modalities' point of view.

between the NC and MCI groups. This allowed the proposed linear-SVM CAD system to succeed in providing the discrimination power between the studied groups. Accordingly, the proposed system showed superior results than the DL that faces under-performance due to the small size of the dataset. Due to the same dataset size, the DT was prone to overfitting since it is considered as a high bias classifier. This fact regarding DT can consequently explain the RF results that could overcome the overfitting problem through constructing a multitude of DTs [53]. Finally, the NB could provide high performance results since it shows good performance with small datasets and it is less influenced by overfitting.

Regarding the prior work, to the best of our knowledge, the presented CAD system described here is the first to present the local/regional diagnosis of AD from different perspectives. Additionally, to the best of our knowledge, it's

the first to combine ^{11}C PiB-PET with sMRI scans to meet the contributed goal. Previous studies have utilized other PET-based data in their combined system but not ^{11}C PiB-PET. Kohannim *et al.* [54] achieved an accuracy of 75.76% when combining sMRI data, FDG-PET, CSF biomarker, ApoE genotype, as well as age. Zhang *et al.* [55] combined sMRI, FDG-PET, and CSF biomarkers to achieve an accuracy of 76.4%. Yu *et al.* [56] also combined sMRI, FDG-PET, and CSF biomarkers to evaluate the same classification problem and achieved an accuracy of 80%.

The proposed system with the fusion data helps to determine the diagnosis specific (MCI) brain regions from structural and functional views which fit into the early involved neurocircuits in MCI/AD. Further the localized diagnoses validates our approach. These brain regions, including the calcarine gyrus (visuospatial skills), left caudate (learning,

F. E.-Z. A. El-Gamal *et al.*: Personalized CAD for MCI in Alzheimer's Disease Based on sMRI and ^{11}C PiB-PET Analysis

IEEE *Access*

memory, motor, language), cerebellum (language, motor), superior frontal gyrus (cognition, executive function), and parahippocampal gyrus (learning, memory, visuospatial, adaptive) have at least modest correlates with connectivity (Tables 4–6) and behaviors affected in MCI subjects. Further the sMRI correlates suggest a widespread early involvement from a structural standpoint and linked to deficits in language, emotions, learning/memory, visual spatial skills, executive function, and adaptive behaviors (Table 4). Besides traditional MCI/AD regions, neuropathological findings of Aβ plaques and neurofibrillary tangles in the cerebellum explains the high retention of ^{11}C PiB-PET in these regions during the early stages of AD/MCI [57]. Clinically, olfactory dysfunction is considered one of the earliest signs of AD [58]. Finally the cingulum is considered one of the earliest imaging abnormality in AD and thus could be an early neurocircuit involved in MCI [59]. Though at an early stage of development, clinicians could use a CAD system to identify early diagnosis of involved MCI neurocircuits and thus consider early personalized treatments, facilitate clinical trials among similar affected subjects, and thereby provide a better infrastructure to discover curative treatments among subgroups of AD/MCI patients.

In the end, it should be noted that proofing the concept of the proposed work by obtaining promising evaluation results encouraged the authors to continue the analysis process in the future in different ways. For example, this encouraged them to evaluate the proposed work on a bigger dataset with more scans for both addressed groups. The results also inspired them to assess the system on other relevant groups to the AD research field (e.g., pMCI and sMCI). Also, it motivated them to evaluate other AD-related modalities to complement the ones utilized in the proposed work.

VI. CONCLUSION

Diagnosing AD at its early stage is a difficult task due to number of reasons, including the variable manifestation of the disease among particular subjects. The proposed study presents a personalized functional/structural based CAD system to help in the early diagnosis of AD, using data from two modalities: ^{11}C PiB-PET, to present a functional diagnosis view, and sMRI, to present a structural perspective. Through a number of analysis steps, the proposed system produced two diagnosis levels. The first level was on the brain regions basis, local/regional diagnosis, to present disease severity in each region from each modality's perspective. Then, integrating the maximum regional results from the two modalities, the second diagnosis level is presented, global diagnosis, that determines whether the subject belongs to the NC or MCI group.

Evaluating the proposed system showed promising results in this pilot study and establishes a proof-of-concept for the proposed framework to address the classification problem of NC vs. MCI. Future work will include evaluating the system on other AD related classification problems (e.g., sMCI *vs.* pMCI, and NC *vs.* AD groups), as well as validation

with a bigger dataset, which could help refine the early neurocircuits involved in MCI subjects. Additionally, other modalities could be evaluated to complement the ones chosen for this study, thereby refining the accuracy, sensitivity, and specificity of localized diagnosis.

REFERENCES

[1] H. Feldman, *Atlas Alzheimer's Disease*, Boca Raton, FL, USA: CRC Press, 2007. [Online]. Available: https://books.google.com/books?id=X5LgkgxgoTMC

[2] (2019). *Alzheimer's Disease International*. Accessed: Apr. 2, 2019. [Online]. Available: https://www.alz.co.uk/

[3] J. Hodler, G. Schulthess, and C. Zollikofer, *Diseases of the Brain, Head & Neck, Spine 2012-2015: Diagnostic Imaging and Interventional Techniques*. Milan, Italy: Springer, 2012.

[4] (2017). *World Health Organization*. Accessed: Mar. 6, 2017. [Online]. Available: http://www.who.int/

[5] S. Gauthier, *Clinical Diagnosis and Management of Alzheimer's Disease*. Boca Raton, FL, USA: CRC Press, 2006.

[6] S. Mordechai, E. Shufan, B. S. Porat Katz, and A. Salman, "Early diagnosis of Alzheimer's disease using infrared spectroscopy of isolated blood samples followed by multivariate analyses," *Analyst*, vol. 142, no. 8, pp. 1276–1284, 2017.

[7] C. R. Jack, D. S. Knopman, W. J. Jagust, L. M. Shaw, P. S. Aisen, M. W. Weiner, R. C. Petersen, and J. Q. Trojanowski, "Hypothetical model of dynamic biomarkers of the Alzheimer's pathological cascade," *Lancet Neurol.*, vol. 9, no. 1, pp. 119–128, Jan. 2010.

[8] K. A. Johnson, S. Minoshima, N. I. Bohnen, K. J. Donohoe, N. L. Foster, P. Herscovitch, J. H. Karlawish, C. C. Rowe, M. C. Carrillo, D. M. Hartley, S. Hedrick, V. Pappas, and W. H. Thies, "Appropriate use criteria for amyloid PET: A report of the amyloid imaging task force, the society of nuclear medicine and molecular imaging, and the Alzheimer's association," *J. Nucl. Med.*, vol. 54, no. 3, pp. 476–490, Mar. 2013.

[9] T. Varghese, R. Sheelakumari, J. S. James, and P. S. Mathuranath, "A review of neuroimaging biomarkers of alzheimer's disease," *Neurol. Asia*, vol. 18, no. 3, p. 239, 2013.

[10] D. Zhang and D. Shen, "Multi-modal multi-task learning for joint prediction of multiple regression and classification variables in Alzheimer's disease," *NeuroImage*, vol. 59, no. 2, pp. 895–907, Jan. 2012.

[11] K. R. Gray, P. Aljabar, R. A. Heckemann, A. Hammers, and D. Rueckert, "Random forest-based similarity measures for multi-modal classification of Alzheimer's disease," *NeuroImage*, vol. 65, pp. 167–175, Jan. 2013.

[12] D. Kim, S. Kim, S. L. Risacher, L. Shen, M. D. Ritchie, M. W. Weiner, A. J. Saykin, and K. Nho, "A graph-based integration of multimodal brain imaging data for the detection of early mild cognitive impairment (e-mci)," in *Proc. Int. Workshop Multimodal Brain Image Anal.* Cham, Switzerland: Springer, 2013, pp. 159–169.

[13] B. Jie, D. Zhang, B. Cheng, and D. Shen, "Manifold regularized multi-task feature selection for multi-modality classification in alzheimer's disease," in *Proc. Int. Conf. Med. Image Comput. Comput.-Assist. Intervent.*, 2013, pp. 275–283.

[14] H.-I. Suk, S.-W. Lee, and D. Shen, "Hierarchical feature representation and multimodal fusion with deep learning for AD/MCI diagnosis," *NeuroImage*, vol. 101, pp. 569–582, Nov. 2014.

[15] M. Liu, D. Zhang, and D. Shen, "Ensemble sparse classification of Alzheimer's disease," *NeuroImage*, vol. 60, no. 2, pp. 1106–1116, Apr. 2012.

[16] M. Liu, D. Zhang, D. Shen, and t. Alzheimer's Disease Neuroimaging Initiative, "Hierarchical fusion of features and classifier decisions for Alzheimer's disease diagnosis," *Hum. Brain Mapping*, vol. 35, no. 4, pp. 1305–1319, Apr. 2014.

[17] L. Lazli, M. Boukadoum, and O. Ait Mohamed, "Computer-aided diagnosis system for Alzheimer's disease using fuzzy-possibilistic tissue segmentation and SVM classification," in *Proc. IEEE Life Sci. Conf. (LSC)*, Oct. 2018, pp. 33–36.

[18] N. Mattsson, P. S. Insel, M. Donohue, J. Jögi, R. Ossenkoppele, T. Olsson, M. Schöll, R. Smith, and O. Hansson, "Predicting diagnosis and cognition with 18 F-AV-1451 tau PET and structural MRI in Alzheimer's disease," *Alzheimer's Dementia*, vol. 15, no. 4, pp. 570–580, Apr. 2019. [Online]. Available: http://www.sciencedirect.com/science/article/pii/S1552526018336057

[19] X. Hao, Y. Bao, Y. Guo, M. Yu, D. Zhang, S. L. Risacher, A. J. Saykin, X. Yao, and L. Shen, "Multi-modal neuroimaging feature selection with consistent metric constraint for diagnosis of Alzheimer's disease," *Med. Image Anal.*, vol. 60, Feb. 2020, Art. no. 101625. [Online]. Available: http://www.sciencedirect.com/science/article/pii/S1361841519301616

[20] R. Li, W. Zhang, H.-I. Suk, L. Wang, J. Li, D. Shen, and S. Ji, "Deep learning based imaging data completion for improved brain disease diagnosis," in *Proc. Int. Conf. Med. Image Comput. Comput.-Assist. Intervent*, 2014, pp. 305–312.

[21] S. Liu, S. Liu, W. Cai, S. Pujol, R. Kikinis, and D. Feng, "Early diagnosis of alzheimer's disease with deep learning," in *Proc. IEEE 11th Int. Symp. Biomed. Imag. (ISBI)*, Dec. 2014, pp. 1015–1018.

[22] H.-I. Suk and D. Shen, "Deep learning-based feature representation for ad/mci classification," in *Medical Image Computing and Computer-Assisted Intervention*, K. Mori, I. Sakuma, Y. Sato, C. Barillot, and N. Navab, Eds. Berlin, Germany: Springer, 2013, pp. 583–590.

[23] M. W. Weiner. (2006). *ADNI 1 Procedures Manual*. [Online]. Available: http://adni.loni.usc.edu/methods/documents/

[24] D. Sohn, K. Shpanskaya, J. E. Lucas, J. R. Petrella, A. J. Saykin, R. E. Tanzi, N. F. Samatova, and P. M. Doraiswamy, "Sex differences in cognitive decline in subjects with high likelihood of mild cognitive impairment due to Alzheimer's disease," *Sci. Rep.*, vol. 8, no. 1, Dec. 2018, Art. no. 7490.

[25] (2020). *ADNI*. Accessed: Apr. 23, 2020. [Online]. Available: http://adni.loni.usc.edu/methods/pet-analysis-method/pet-analysis/

[26] H. Matsuda, T. Asada, and A. Tokumaru, *Neuroimaging Diagnosis for Alzheimer's Disease Other Dementias*. Tokyo, Japan: Springer, 2017. [Online]. Available: https://books.google.com.eg/books?id=FEwzDwAAQBAJ

[27] (2020). *Adni*. Accessed: Apr. 23, 2020. [Online]. Available: http://adni.loni.usc.edu/methods/mri-tool/mri-pre-processing/

[28] W. NeuroImaging. (2017). *Spm12—Statistical Parametric Mapping*. Accessed: Nov. 7, 2017. [Online]. Available: http://www.fil.ion.ucl.ac.uk/spm/software/spm12/

[29] T. Briand and P. Monasse, "Theory and practice of image B-Spline interpolation," *Image Process. Line*, vol. 8, pp. 99–141, Jul. 2018.

[30] M. Taleb and E. McKay, "Evaluation of the mutual information cost function for registration of SPET and MRI images of the brain," *Nucl. Med. Commun.*, vol. 20, no. 4, p. 385, Apr. 1999.

[31] J. Ashburner and K. J. Friston, "Unified segmentation," *NeuroImage*, vol. 26, no. 3, pp. 839–851, Jul. 2005. [Online]. Available: http://www.sciencedirect.com/science/article/pii/S1053811905001102

[32] S. Agrawal and Y. Bahendwar, "A comparative analysis of thresholding techniques for denoising of MRI image using wavelets," *Res. J. Eng. Technol.*, vol. 3, no. 1, pp. 34–37, 2012.

[33] Y. S. Bahendwar and G. Sinha, "A comparative performance analysis of discrete wavelet transforms for denoising of medical images," in *CAD/CAM, Robotics Factories Future*. New Delhi, India: Springer, 2016, pp. 417–424.

[34] M. Vallières, C. R. Freeman, S. R. Skamene, and I. El Naqa, "A radiomics model from joint FDG-PET and MRI texture features for the prediction of lung metastases in soft-tissue sarcomas of the extremities," *Phys. Med. Biol.*, vol. 60, no. 14, p. 5471, 2015.

[35] U. Bagci and D. J. Mollura, "Denoising pet images using singular value thresholding and stein's unbiased risk estimate," in *Proc. Int. Conf. Med. Image Comput. Comput.-Assist. Intervent.*, 2013, pp. 115–122.

[36] S.-S. Su, K.-W. Chen, and Q. Huang, "Discriminant analysis in the study of Alzheimer's disease using feature extractions and support vector machines in positron emission tomography with 18F-FDG," *J. Shanghai Jiaotong Univ.*, vol. 19, no. 5, pp. 555–560, Oct. 2014.

[37] Y. Zhang, Z. Dong, P. Phillips, S. Wang, G. Ji, J. Yang, and T.-F. Yuan, "Detection of subjects and brain regions related to Alzheimer's disease using 3D MRI scans based on eigenbrain and machine learning," *Frontiers Comput. Neurosci.*, vol. 9, p. 66, Jun. 2015.

[38] D. Salas-Gonzalez, F. Segovia, F. J. Martínez-Murcia, E. W. Lang, J. M. Gorriz, and J. Ramlrez, "An optimal approach for selecting discriminant regions for the diagnosis of Alzheimer's disease," *Current Alzheimer Res.*, vol. 13, no. 7, pp. 838–844, May 2016.

[39] N. Tzourio-Mazoyer, B. Landeau, D. Papathanassiou, F. Crivello, O. Etard, N. Delcroix, B. Mazoyer, and M. Joliot, "Automated anatomical labeling of activations in SPM using a macroscopic anatomical parcellation of the MNI MRI single-subject brain," *NeuroImage*, vol. 15, no. 1, pp. 273–289, Jan. 2002.

[40] C. Turkington and D. Mitchell, *The Encyclopedia Alzheimer's Disease* (Facts on File Library of Health & Living). New York, NY, USA: Facts On File, 2010. [Online]. Available: https://books.google.com/books?id=SA2X3ZHUZaEC

[41] C. Kumar and A. Kumari, "3D reconstruction of brain tumor from 2D MRI's using FCM and marching cubes," *Int. J. Adv. Res. Electron. Commun. Engin.*, vol. 3, no. 9, pp. 970–974, 2014.

[42] D. Castillo-Barnes, F. J. Martinez-Murcia, A. Ortiz, D. Salas-Gonzalez, J. Ramìrez, and J. M. Górriz, "Morphological characterization of functional brain imaging by isosurface analysis in Parkinson's disease," *Int. J. Neural Syst.*, vol. 30, no. 9, Sep. 2020, Art. no. 2050044.

[43] A. Ortiz, J. Munilla, M. Martínez-Ibañez, J. M. Górriz, J. Ramírez, and D. Salas-Gonzalez, "Parkinson's disease detection using isosurfaces-based features and convolutional neural networks," *Frontiers Neuroinform.*, vol. 13, p. 48, Jul. 2019. [Online]. Available: https://www.frontiersin.org/article/10.3389/fninf.2019.00048

[44] T. S. Newman and H. Yi, "A survey of the marching cubes algorithm," *Comput. Graph.*, vol. 30, no. 5, pp. 854–879, Oct. 2006.

[45] P. Vemuri and C. R. Jack, "Role of structural MRI in Alzheimer's disease," *Alzheimer's Res. Therapy*, vol. 2, no. 4, p. 23, Aug. 2010, doi: 10.1186/alzrt47.

[46] M. Haghighat, M. Abdel-Mottaleb, and W. Alhalabi, "Fully automatic face normalization and single sample face recognition in unconstrained environments," *Expert Syst. Appl.*, vol. 47, pp. 23–34, Apr. 2016. [Online]. Available: http://www.sciencedirect.com/science/article/pii/S0957417415007514

F. E.-Z. A. El-Gamal *et al.*: Personalized CAD for MCI in Alzheimer's Disease Based on sMRI and ^{11}C PiB-PET Analysis

IEEE Access

[47] F. E. A. El-Gamal, M. M. Elmogy, M. Ghazal, A. Atwan, M. F. Casanova, G. N. Barnes, R. Keynton, A. S. El-Baz, and A. Khalil, "A novel early diagnosis system for mild cognitive impairment based on local region analysis: A pilot study," *Frontiers Human Neurosci.*, vol. 11, p. 643, Jan. 2018. [Online]. Available: https://www.frontiersin.org/article/10.3389/fnhum.2017.00643

[48] K. D. Toennies, *Guide to Medical Image Analysis: Methods and Algorithms*. Cham, Switzerland: Springer, 2012.

[49] J. Shin, S.-Y. Lee, S. J. Kim, S.-H. Kim, S.-J. Cho, and Y.-B. Kim, "Voxel-based analysis of Alzheimer's disease PET imaging using a triplet of radiotracers: PIB, FDDNP, and FDG," *NeuroImage*, vol. 52, no. 2, pp. 488–496, Aug. 2010. [Online]. Available: http://www.sciencedirect.com/science/article/pii/S1053811910004076

[50] (2017). *Xjview|a Viewing Program for SPM.* Accessed: Jan. 23, 2017. [Online]. Available: http://www.alivelearn.net/xjview/

[51] Y. Zhang, S. Wang, and Z. Dong, "Classification of alzheimer disease based on structural magnetic resonance imaging by kernel support vector machine decision tree," *Prog. Electromagn. Res.*, vol. 144, pp. 171–184, Dec. 2014.

[52] L. Khedher, J. Ramírez, J. M. Górriz, and A. Brahim, "Automatic classification of segmented MRI data combining independent component analysis and support vector machines," in *Innovation in Medicine and Healthcare* (Studies in Health Technology and Informatics). Amsterdam, The Netherlands: IOS Press, 2014, pp. 271–279.

[53] J. Park, H. Jin, Y. Jeong, and M. Khan, *Advanced Multimedia and Ubiquitous Engineering: FutureTech & MUE* (Lecture Notes in Electrical Engineering). Singapore: Springer, 2016. [Online]. Available: https://books.google.com/books?id=L8TsDAAAQBAJ

[54] O. Kohannim, X. Hua, D. P. Hibar, S. Lee, Y.-Y. Chou, A. W. Toga, C. R. Jack, M. W. Weiner, and P. M. Thompson, "Boosting power for clinical trials using classifiers based on multiple biomarkers," *Neurobiol. Aging*, vol. 31, no. 8, pp. 1429–1442, Aug. 2010.

[55] D. Zhang, Y. Wang, L. Zhou, H. Yuan, and D. Shen, "Multimodal classification of Alzheimer's disease and mild cognitive impairment," *NeuroImage*, vol. 55, no. 3, pp. 856–867, 2011. [Online]. Available: http://www.sciencedirect.com/science/article/pii/S1053811911000267

[56] G. Yu, Y. Liu, and D. Shen, "Graph-guided joint prediction of class label and clinical scores for the Alzheimer's disease," *Brain Struct. Function*, vol. 221, no. 7, pp. 3787–3801, Sep. 2016, doi: 10.1007/s00429-015-1132-6.

[57] L. Baldaçara, J. G. F. Borgio, W. A. D. S. Moraes, A. L. T. Lacerda, M. B. M. M. Monta no, S. Tufik, R. A. Bressan, L. R. Ramos, and A. P. Jackowski, "Cerebellar vol. in, patients with dementia," *Revista Brasileira de Psiquiatria*, vol. 33, no. 2, pp. 122–129, 2011.

[58] Y. M. Zou, D. Lu, L. P. Liu, H. H. Zhang, and Y. Y. Zhou, "Olfactory dysfunction in Alzheimer's disease," *Neuropsychiatric Disease Treat.*, vol. 12, pp. 869–875, Dec. 2016.

[59] L. Rami, R. Sala-Llonch, C. Solé-Padullés, J. Fortea, J. Olives, A. Lladó, C. Peña-Gómez, M. Balasa, B. Bosch, A. Antonell, R. Sanchez-Valle, D. Bartrés-Faz, and J. L. Molinuevo, "Distinct functional activity of the precuneus and posterior cingulate cortex during encoding in the preclinical stage of Alzheimer's disease," *J. Alzheimer's Disease*, vol. 31, no. 3, pp. 517–526, Aug. 2012.

MOHAMMED M. ELMOGY (Senior Member, IEEE) received the B.Sc. and M.Sc. degrees from the Faculty of Engineering, Mansoura University, Mansoura, Egypt, and the Ph.D. degree from the Department of Informatics, MIN Faculty, Hamburg University, Hamburg, Germany, in 2010.

He worked as a Visiting Researcher with the Department of Bioengineering, University of Louisville, Louisville, KY, USA, from July 2016 to August 2019. He is currently an Associate Professor with the Department of Information Technology, Faculty of Computers and Information, Mansoura University. He has authored/coauthored over 200 research publications in peer-reviewed reputed journals, book chapters, and conference proceedings. He advised more than 30 master and doctoral graduates. His current research interests include computer vision, medical image analysis, machine learning, pattern recognition, and biomedical engineering. He has served as a reviewer for various international journals. He has also served as a technical program committee member in many workshops and conferences. He is also a Professional Member of ACM Society.

ASHRAF KHALIL received the Ph.D. degree in computer science from Indiana University, USA. He is currently a Professor with the College of Technological Innovation, Zayed University, United Arab Emirates. He has published notable research in ubiquitous computing, social and mobile computing, bioinformatics, persuasive computing, and human–computer interaction. The results of his research are published in the top conferences in the field, such as CHI, CSCW, and INTERACT. He has authored over 50 publications in top journals and conferences and achieved numerous accolades including many research grants from ADEK, Emirates Foundation, and Google. He has served as a usability consultant for major companies, such as Nokia, HSBC, and Samsung. He is interested in applying diverse technological innovations in addressing pertinent problems.

MOHAMMED GHAZAL (Senior Member, IEEE) received the B.Sc. degree in computer engineering from the American University of Sharjah (AUS), in 2004, and the M.A.Sc. and Ph.D. degrees in electrical and computer engineering (ECE) from Concordia University, Montreal, QC, Canada, in 2010 and 2006, respectively.

He is currently an Associate Professor and the Chair of ECE with Abu Dhabi University and an Adjunct Associate Professor of bioengineering with the University of Louisville. He has authored or coauthored over 40 publications in recognized international journals and conferences, including the IEEE TRANSACTIONS ON IMAGE PROCESSING, the IEEE TRANSACTIONS ON CIRCUITS AND SYSTEMS FOR VIDEO TECHNOLOGY, the IEEE TRANSACTIONS ON CONSUMER ELECTRONICS, *Renewable and Sustainable Energy Reviews* (Elsevier), and *Multimedia Tools and Applications* (Springer). His research interests include bioengineering, image and video processing, and smart systems. He is also a member of ACM and BMES. He was a recipient of multiple awards, including the Distinguished Faculty Award of Abu Dhabi University, in 2017 and 2014, a Special Innovation Award of AED 1 000 000 by the Office of Prime Minister of the UAE, the NSERC's Alexander Graham Bill's Scholarship, AUS's Presidents Cup, and the Ministry of Education Shield for Creative Thinking.

FATMA EL-ZAHRAA A. EL-GAMAL received the B.Sc. and M.Sc. degrees in information technology (IT) from the Faculty of Computers and Information, Mansoura University, Egypt, in 2010 and 2013, respectively.

She worked as a Demonstrator with the Faculty of Computers and Information from 2011 to 2013, and as a Teacher Assistant from 2014 to 2016. She was a Ph.D. Visiting Scholar with the Department of Bioengineering, University of Louisville, Louisville, KY, USA, from 2016 to 2019. She is currently a Lecturer with the Department of IT, Faculty of Computers and Information, Mansoura University. Her research interests include biomedical engineering, computer vision, image processing, pattern recognition, and machine learning.

JAWAD YOUSAF (Senior Member, IEEE) received the M.S. and Ph.D. degrees in electronics and electrical engineering from Sungkyunkwan University, Suwon, South Korea, in 2016 and 2019, respectively. He worked as the Brain of Korea (BK)-Postdoctoral Fellow with the EMC Laboratory, Sungkyunkwan University, from March 2019 to July 2019. He is currently working as an Assistant Professor with the Department of Electrical and Computer Engineering, Abu Dhabi University, United Arab Emirates. Also, he worked as the Senior RF Researcher with the Pakistan Space and Upper Atmosphere Research Commission (SUPARCO: National Space Agency of Pakistan), from 2009 to 2013. His research interests include artificial intelligence, ESD analysis, chipless RFID tags, and EMI/EMC analysis of the systems for space and commercial environment. His research work has results in over 50 publications in leading peer reviewed international technical journals, and referred international and national conferences. He was a recipient of prestigious Brain of Korea (BK)-21 Postdoctorate Fellowship 2019, 2nd Best Ph.D. Graduate Award of Collage 2019, Best Paper Award in 49th KIEE Summer Conference 2018, winner of the Grand Prize for Best Paper in 3rd Electromagnetic Measurement Competition of KIESS 2018, Prestigious Annual EMC Scholarship Award of KIEES and EMCIS Company Ltd. 2017, Best EMC Symposium Paper Award, and EDCOM Best Student Paper Award Finalist in 2017 IEEE International Symposium on EMC and SI/PI 2017 (USA).

XIAOLU QIU received the bachelor's and M.D. degrees from Nanchang University. From 2017 to 2019, she was a Visiting Clinical Scholar and a Researcher with the University of Louisville Autism Center, USA. She is currently a Developmental Pediatrician and a Neurological Researcher with Jiangxi Children's Hospital in Nanchang, China. Her clinical interests include the early diagnosis and management of autism spectrum disorder. Her research interests include the use of multimodal MRI in children and adults with neurological disorders.
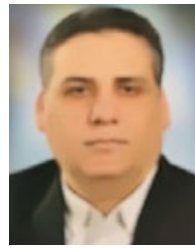
HASSAN H. SOLIMAN received the B.Sc., M.Sc., and Ph.D. degrees in electronics and communications engineering from the Faculty of Engineering, Mansoura University, Mansoura, Egypt, in 1983, 1987, and 1993, respectively. He worked as an Assistant Professor, an Associate Professor, and a Professor with the Faculty of Engineering, Mansoura University, from 1993 to 2016. From 1999 to 2002, he worked as a Visiting Associate Professor with the Department of Computer and Information, College of Telecom and Information, Riyadh, Saudi Arabia. In 2004 to 2009, he worked as a Visiting Associate Professor with the Department of Computer and Information, Taibah University, Saudi Arabia. He has been a Professor with the Information Technology and since 2015, he has also been working as a Dean of the Faculty of Computers and Information, Mansoura University. He has authored/coauthored over 50 research publications in peer-reviewed reputed journals, book chapters, and conference proceedings. He advised more than 20 master and doctoral graduates. His current research interests include computer networking, computer security, medical image analysis, and machine learning.

AHMED ATWAN received the B.Sc., M.Sc., and Ph.D. degrees in electronics and communications engineering from the Faculty of Engineering, Mansoura University, Egypt, in 1988, 1998, and 2004, respectively. From 2000 to 2004, he worked as a Lecturer with the Faculty of Technology, Al Bahah, Saudi Arabia. From 2005 to 2009, he worked as an Assistant Professor with the Faculty of Computers and Information Sciences (FCIS), Mansoura University. From 2010 to 2015, he worked as an Associate Professor with FCIS, Mansoura University. Since 2016, he has been working as a Professor with FCIS, Mansoura University. Since 2019 until now, he has also been working as a Professor with the Faculty of Computer and Information Technology, Northern Boarder University, Saudi Arabia. His research interests include pattern recognition, networking, signal processing, and image processing.

HERMANN B. FRIEBOES received the Ph.D. degree in biomedical engineering from the University of California, Irvine, in 2006. He is currently an Associate Professor with the Department of Bioengineering, University of Louisville. His research interests include the interdisciplinary development and implementation of mathematical modeling, computational simulation, and experimental biology techniques that can be quantitatively integrated to characterize disease progression and treatment response. This work includes the development of quantitative techniques for multiscale linking of the molecular- to cell- to-tissue-scale interactions and associated biophysical processes during disease progression. He is the author of numerous peer-reviewed journal articles and book chapters, and his work has been supported by grant funding from the National Institutes of Health.

GREGORY NEAL BARNES is currently the Inaugural Permanent Director of the University of Louisville Autism Center. He also holds the Spafford Ackerly Chair for Child and Adolescent Psychiatry and faculty positions in the Departments of Neurology and Pediatrics. His research interests include potential genetic influences into the development of ASD and epilepsy and how these factors contribute to outcomes and potential new treatments. He is also a UL Professor of neurology and pediatrics, has held academic appointments at the Washington University School of Medicine in St. Louis, the Harvard Medical School, the Duke University Medical School, the University of Kentucky College of Medicine, and the Vanderbilt School of Medicine. He has authored or coauthored 58 research articles/book chapters in the fields of neurology, autism, and epilepsy. He also serves as a PI of several national multi-site grants to understand the role of cannabinoid signaling in autism.

AYMAN S. EL-BAZ (Senior Member, IEEE) received the bachelor's and master's degrees in electrical engineering, in 1997 and 2001, respectively, and the Ph.D. degree in electrical engineering from the University of Louisville, Louisville, KY, USA, in 2006. He is currently a Professor with University Scholar, and the Chair of the Department of Bioengineering, University of Louisville. In 2009, he was named as a Coulter Fellow for his contributions to the field of biomedical translational research. He has 15 years of hands-on experience in the fields of bio-imaging modeling and non-invasive computer-assisted diagnosis systems. He has authored or coauthored more than 450 technical articles (105 journals, 15 books, 50 book chapters, 175 refereed-conference papers, 100 abstracts, and 15 U.S. patents).